Kinetics of Polystyrene Adsorption onto Gold from Dilute Θ Solutions

T. Z. Fu,† U. Stimming,‡ and C. J. Durning*

Department of Chemical Engineering & Applied Chemistry, Columbia University, New York, New York 10027

Received July 21, 1992; Revised Manuscript Received March 18, 1993

ABSTRACT: A quartz crystal microbalance (QCM) was applied to study the kinetics of adsorption of nearly monodisperse, high molecular weight polystyrene (PS) onto gold from dilute solutions at the Θ condition. An analysis of QCM frequency shifts during adsorption, based on the mechanical resonance theory of Kanazawa et al.,[24,25] predicts that the shift is proportional to a linear combination of the adsorbed layer depth and the polymer coverage. A method is proposed to extract the portion of the shift due to the coverage, which enables one to construct the expected isotherm from equilibrium frequency shifts. The effects on the adsorption kinetics of polymer molecular weight and of bulk polymer concentration were studied systematically. The data were compared to a preliminary theory by de Gennes[5,6] which assumes that an adsorbed layer relaxes instantaneously during adsorption and that the adsorption rate is controlled by end-in reptation of chains across the partially developed layer. The data deviate from the theory in two ways. Firstly, the adsorption process has a much longer time scale than any realistic estimate based on the end-in reptation mechanism, and this time scale is insensitive to molecular weight, which is at odds with prediction. Secondly, the transmission coefficient of a partially formed adsorbed layer clearly depends on how the layer was formed, suggesting that memory effects play an important role in the layer formation process. In toto, the kinetic data suggest that long time scale surface rearrangements insensitive to molecular weight control the adsorption rate in this system.

1. Introduction

A good understanding of polymer adsorption lies at the heart of advancing many applications in colloid science and lubrication.[1] Based of this, considerable attention has been focused on the fundamentals of the process over the last three decades. Three extensive reviews[2–4] summarize the work through 1987. Although significant progress has been achieved, a full comprehension of polymer adsorption, especially of its kinetic aspects, has not yet been realized.

In this work we focus on the kinetics of adsorption of linear, nearly monodisperse, flexible chains from dilute solutions onto a flat, attractive surface. We used a quartz crystal microbalance (QCM) in a systematic investigation of the influences of chain length and of bulk polymer concentration. The data permit a preliminary test of the end-in reptation mechanism for adsorption proposed recently by de Gennes.[5,6]

In the remainder of this section, we summarize a few well established facts about the adsorption process. Then, de Gennes's picture of the adsorption kinetics is summarized. Subsequent to that, we give an interpretation of what the QCM measures during adsorption and then present the experimental details. Finally, we compare the experimental results to the preliminary theoretical predictions.

Many experimental techniques have been employed to study polymer adsorption: ellipsometry,[7] surface forces measurements,[8] attenuated total reflectance infrared spectroscopy,[9] radiotracer techniques,[10] and neutron scattering.[11] To quickly review some of the well-known aspects of polymer adsorption, consider the results of the ellipsometric studies by Takahashi et al.[7] With ellipsometry, one measures both the polymer coverage, Γ (monomers/cm^2), and the depth of the adsorbed layer, R. Takahashi et al. studied polystyrene (PS) adsorption onto chrome from dilute Θ solutions (cyclohexane at 35 °C) and from solutions in a good solvent (toluene at 35 °C). Regarding the adsorption isotherm, they observed a bulk concentration c_{sat} below which Γ_e and R_e (the equilibrium values of Γ and R) increase with bulk polymer concentration, c_b, but above which Γ_e and R_e saturate. The saturation value of R_e, R_{sat}, is the same order of magnitude and has the same dependence on polymer molecular weight as the coil radius in dilute solution, R_F. The saturation value of Γ_e, Γ_{sat}, shows only a weak molecular weight dependence for high enough molecular weights (>10^5 for PS). These basic equilibrium features can be explained neatly by the scaling theory summarized in the next section.

Takahashi et al. also observed the kinetics of both Γ and R for $c_b > c_{sat}$. The kinetic data are not extensive, but an obvious feature is that R reaches its equilibrium value much faster than does Γ; typically, the latter develops over a time scale nearly 1 order of magnitude longer than that for R. This observation suggests that a nascent adsorbed layer forms relatively quickly and subsequently densifies at nearly constant depth by the slow incorporation of new chains into the adsorbed layer.

2. Theoretical Background

2.1. Scaling Theory for Equilibrium States. de Gennes'[5,6] discussion of adsorption kinetics draws heavily on a scaling analysis of polymer adsorption equilibria. Bouchaud and Dauod[12] summarize the calculation of the adsorption isotherm for monodisperse, flexible chains adsorbed from good solvents onto flat, attractive surfaces. The analysis predicts three regimes of surface coverage: two-dimensional dilute, two-dimensional semidilute, and a "plateau" regime. In the first two regimes, Γ_e increases linearly with c_b; in the plateau regime there is practically no change in Γ_e with c_b.

In the two-dimensional, dilute regime, each adsorbed chain is isolated on the surface. The equilibrium thickness of the adsorbed layer, d, obeys $d \cong \delta^{-1}a$ where δkT is the

* To whom correspondences should be sent.
† Current address: International Paper Co., Corporate Research Center, Tuxedo, NY 10987.
‡ Current address: Institute of Energy Process Engineering, Juelich Research Center, 5170 Juelich, Germany.

0024-9297/93/2226-3271$04.00/0 © 1993 American Chemical Society

sticking energy for a segment on the surface and a is the segment length. Note that if $\delta \sim O(1)$, meaning relatively strong adsorption, then $d \cong a$, meaning that each chain sticks quite flat. The coil's extension parallel to the surface, $R_\parallel$, obeys the law for a two-dimensional, self-avoiding walk: $R_\parallel \cong a\delta^{1/4}N^{3/4}$ where N is the number of segments per chain. The surface layer remains dilute as long as Γ_e is smaller than a surface overlap threshold, Γ_1^*, deduced from $R_\parallel$ as $\Gamma_1^* \cong a^{-2}(N\delta)^{-1/2}$. Deriving the adsorbed chain free energy and enforcing the condition for phase equilibrium leads to a linear relationship between Γ_e and c_b in this regime which indicates that for $\delta \sim O(1)$ (strong adsorption) adsorbed chains begin to overlap for very dilute bulk solutions ($c_b \ll c^*$).

For $\Gamma_e > \Gamma_1^*$ adsorbed chains begin to overlap laterally and a semidilute adsorbed layer emerges. Consideration of the free energy per adsorbed chain shows that as long as $\Gamma_e < \Gamma_2^*$ the excluded volume contributions from lateral overlap could be neglected; consequently, a linear isotherm still remains valid in this regime. The bulk concentration corresponding to Γ_2^*, c_{b2}^*, lies well below c* for high molecular weight polymers.

For $c_b > c_{b2}^*$ the character of the isotherm changes drastically. Here the interchain excluded volume part in the adsorbed chain free energy cannot be neglected when determining the isotherm. The conditions for phase equilibrium give

$$\Gamma_e \cong (\delta^{1/3}/a^2)[1 + \kappa(c_b,N,\delta)]; \quad \Gamma_e > \Gamma_2^*, \quad \text{good solvents} \tag{2.1}$$

where $|\kappa| \ll 1$ and $\kappa \sim 1/N$. This indicates that c_{b2}^* is, essentially, c_{sat}, and that Γ_{sat} is nearly independent of N for large N. Consequently when $\delta \sim O(1)$ and N is large, Γ_1^*/Γ_{sat} ($\cong\delta^{-5/6}N^{-1/2}$) is expected to be very small and $\Gamma_2^*/\Gamma_{sat} \cong 1$. This means that the interval (Γ_1^*, Γ_2^*) constitutes the majority of the span in Γ_e for strongly adsorbed high molecular weight polymers. All of the foregoing predictions concerning the isotherm are in essential agreement with experiment.[3,4]

de Gennes[13] studied the plateau regime in detail by a variational method. He worked out the monomer density profiles for high molecular weight polymer strongly adsorbed from good solvent and proposed a simple fractal construction to describe the structure of the major (central) portion of the profile. According to ref 13, the local screening length in the central portion of the adsorbed layer adjusts to the normal distance from the surface. This implies the monomer density profile in the central portion $\phi(z) \cong (z/a)^{-4/3}$ for strong adsorption from good solvents where ϕ is the local polymer volume fraction, which has been verified in a neutron scattering study.[11]

The foregoing analyses focused on good solvents but the results can be adapted to the case of Θ solvents. Since the interchain excluded volume effects are neglected when calculating the isotherms in both the two-dimensional dilute and semidilute regimes, it is clear that the calculation in ref 12 for these regimes remains valid for Θ conditions, although the exponents employed in the scaling analysis must be modified to reflect the absence of intrachain excluded volume. Similarly, de Gennes'[13] fractal construction for the monomer density profile in the plateau regime can be applied for the Θ case. The central portion of the concentration profile should obey

$$\phi(z) \cong a/z;$$

$$\delta \sim O(1), \quad a < z < R_F, \quad \Theta \text{ solvents}, \quad c_b > c_{sat} \tag{2.2}$$

in the case of strong adsorption ($\delta \sim O(1)$). Both $\Gamma_{sat}(N,c_b > c_{sat})$ and $R_{sat}(N,c_b > c_{sat})$ are implied by eq 2.2 and the resulting predictions are in essential agreement with experiment.

2.2. Theory of Adsorption Kinetics. de Gennes[5,6] analyzed adsorption kinetics for monodisperse, flexible chains adsorbing from dilute solutions in good solvents onto a flat solid/liquid interface. In this section we summarize his ideas and make appropriate changes for the case of Θ solvents. The main simplifying assumption adopted in ref 5, termed adiabatic growth, is of fast relaxation on the surface during adsorption. According to ref 5, for $c_b > c_1^*$, the adsorption process onto an initially clean surface has three major stages. Initially, there are no chains on the adsorbing surface; incoming chains stick and, for adiabatic growth, quickly rearrange into an expanded pancake with $R_\parallel \sim N^{3/4}$ before being perturbed by other incoming chains. For a high molecular weight polymer, this regime is limited to very low surface coverages, $\Gamma < \Gamma_1^*$. As time progresses the coverage exceeds Γ_1^* and a second stage begins. Adsorbed chains begin to compete for adsorption sites; loops and tails begin to appear, and a "fluffy" layer is formed. An important feature emerges during this stage; the barrier effect of the partially formed layer against the incoming chains. It may also occur that the adsorbed layer can glassify near the adsorbing surface.[14,15] This would slow down rearrangements within the adsorbed layer, possibly invalidating the assumption of adiabatic growth, but this possibility is ignored in ref 5. Ultimately, when the adsorbed layer is very close to equilibrium ($1-\Gamma/\Gamma_e \ll 1$) a third stage appears where a dynamic exchange between free chains in solution and adsorbed chains begins, with the incoming and outgoing fluxes nearly in balance.

For systems of practical interest, the most important stage is the second. In such cases, the molecular weight is large ($N \gg 1$), the segment sticking energy is moderate ($\delta \sim O(1)$) and the bulk concentration exceeds c_{sat}, so that for adiabatic conditions the second stage persists for $\epsilon < \Gamma/\Gamma_e < 1-\epsilon$ where $\epsilon \ll 1$; i.e. the second stage spans the majority of the range in Γ. de Gennes showed that if the second stage proceeds adiabatically, then the partially formed layer has the same fractal structure discussed above, but truncated at a nonequilibrium depth $R < R_e$. Therefore, assuming $\delta \sim O(1)$, the growing layer presumably has the concentration distribution $\phi(z) \cong a/z$ for $a \le z \le R < R_e$ in Θ solvents.

Now, the rate of accumulation of adsorbed monomers, $d\Gamma/dt$, equals the difference between the flux from bulk to inside the layer, J_{si}, and the exit flux from inside to the bulk, J_{is}. If the barrier effect near the surface dominates, J_{si} has a form reminiscent of that for a Nernst diffusion layer; de Gennes adopted

$$J_{si} = K_{si}(\Gamma)\beta(\Gamma)c_b \tag{2.3}$$

where K_{si} is the Nernst transmission coefficient characterizing diffusive transport of segments across the adsorbed layer and $\beta(\Gamma)$ is a statistical weight accounting for the repulsive barrier caused by excluded volume in the layer. The exit flux J_{is} is written

$$J_{is} = K_{is}\Gamma R^{-1} \tag{2.4}$$

where Γ/R is the mean monomer concentration in the layer and $K_{is}(\Gamma)$ is related to $K_{si}(\Gamma)$ so as to ensure that the correct equilibrium isotherm results when one puts $d\Gamma/dt = 0$.

In order to specify the coefficients $K_{si}(\Gamma)$ and $\beta(\Gamma)$, one must specify the mechanism governing the incorporation

of a chain into the adsorbed layer. According to refs 5 and 6, this occurs in two sequential steps. First, an incoming chain reptates end-in toward the surface against friction in the layer and, for good solvents, a repulsive excluded-volume barrier, in order to make a first contact with the surface. After entry, the chain "spreads" into a low free energy conformation on the surface. The spreading process, driven by the difference in adsorbed-segment chemical potentials between the partially formed and equilibrium layers, occurs against friction near the adsorbing wall. Assuming that reptative motion governs both processes, the time scales of entry, τ_e, and spreading, τ_s, for a layer very close to equilibrium were calculated in ref 6 for good solvent conditions. The calculation showed that if there is no enhancement of friction near the wall, entry should limit during the second stage for large N. Adapting these results to the Θ case leads to the same expectation.

From the appropriate expression for $K_{is}(\Gamma)$, one finds that during the second stage the exit flux J_{is} is very small relative to the influx, J_{si}. Consequently, one has a condensed form for $d\Gamma/dt$:

$$d\Gamma/dt \cong K_{si}(\Gamma)\beta(\Gamma)c_b;$$

$$\Gamma_1^* < \Gamma < \Gamma_e \text{ for } \Gamma_e < \Gamma_2^* \text{ and } \Gamma_1^* < \Gamma < \Gamma_2^* \text{ for } \Gamma_e > \Gamma_2^* \quad (2.5)$$

For Θ solvents excluded-volume effects are weak so $\beta(\Gamma) = 1$, and if entry is rate limiting, one can set the Nernst coefficient $K_{si}(\Gamma) = D(\Gamma)/R(\Gamma)$ where D is a translational diffusion coefficient for segments to cross the partially formed layer, a process controlled by end-in reptation. According to ref 6

$$D(\Gamma) \cong (kT/N^2f_s)\ln(g(R(\Gamma))) = D_o \ln(R(\Gamma)/a) \quad (2.6)$$

where $g(R)$ means the number of monomers in a loop of size $R(= (R/a)^{1/\nu}$ where ν is the Flory exponent) and $D_o = kT/N^2f_s\nu$ with f_s being the monomeric friction coefficient relevant to the adsorbed layer. To determine $R(\Gamma)$ we note $(\Gamma_e - \Gamma) \equiv \Gamma_e x \cong \int_R^{R_e} a^{-3}\phi(z)\,dz$ which leads to

$$R \cong R_e e^{-\gamma_e x}; \quad \Theta \text{ solvents} \quad (2.7)$$

for Θ conditions when eq 2.2 is used for $\phi(z)$. Here, $\gamma_e \equiv a^2\Gamma_e \cong a^{-1}\int_a^{R_e}\phi(z)\,dz = \ln(R_e/a)$. Note that eq 2.7 gives correct limits for the initial state ($R \to a$ as $x \to 1$) and for the final state ($R \to R_e$ as $x \to 0$). This relationship, a direct consequence of the adiabatic growth assumption, asserts an exponential relationship between R and Γ during adsorption from Θ solvents, the same that one would expect for R_e vs Γ_e in equilibrated layers. This expression is qualitatively consistent with the predictions for $R_e(\Gamma_e)$ from the Scheutjens–Fleer mean-field theory at low bulk concentrations[3,16a,b] and with experimental measurements on equilibrated systems.[16b,c]

Now, introducing eqs 2.6 and 2.7 into eq 2.5, and approximating the weak log term by $\ln(R_e/a)$ gives for Θ conditions

$$d\Gamma/dt = -\Gamma_e dx/dt \simeq K_e c_b e^{\gamma_e x}; \quad \Theta \text{ solvents} \quad (2.8)$$

where the same restrictions on Γ apply as in eq 2.5. Here, $K_e = (D_o/R_e)\ln(R_e/a)$ is the transmission coefficient for the final equilibrated layer. The reader should note that this expression does not have the proper limiting behaviors for the initial and final states ($x = 1$ and $x = 0$, respectively). Initially, there is no adsorbed layer and adsorption is likely controlled by bulk diffusion to the surface. In the diffusion-controlled limit $d\Gamma/dt$ should diverge initially.[17] This discrepancy can be ignored however, since it exists for only a short time scale and a narrow span of coverage in cases of interest. Further, the initial value of $d\Gamma/dt$ from eq 2.8 is very large, $(d\Gamma/dt)_o \cong K_e c_b R_e/a \sim D_o c_b/a$, and should provide a reasonable, albeit fictitious, initial condition. For the final state ($x = 0$), eq 2.8 gives a finite flux, $(d\Gamma/dt)_e = K_e c_b$. This mistake stems from neglecting the back-current, J_{is}, and indicates that one cannot apply eq 2.8 very close to equilibrium.

For strong adsorption ($\delta \sim O(1)$) it is likely that γ_e exceeds unity for very high molecular weight polymer (e.g. eq 2.7 implies $\gamma_e \cong \ln(R_e/a) \sim \ln N$, which diverges weakly with N). So, we are encouraged to simplify eq 2.8 by letting γ_e be large. Doing this leads to the simple law

$$\Gamma/\Gamma_e = (1 - x) \cong 1 + \gamma_e^{-1}\ln(t/\theta + e);$$

$$N \gg 1, \delta \sim O(1), \gamma_e \gg 1, x \sim O(1), \Theta \text{ solvent} \quad (2.9)$$

where $\theta = (a^2K_e c_b)^{-1} = R_e/(a^2D_o c_b \ln(R_e/a))$ is a molecular weight dependent characteristic time and $e = e^{-\gamma_e}$ is presumed to be small. Obviously, eq 2.9 breaks down when x approaches zero.

Equation 2.9 predicts for the majority of the adsorption process that the coverage develops logarithmically in time, with a characteristic time θ depending strongly on molecular weight

$$\theta \sim N^{5/2}/(c_b \ln N) \quad (2.10)$$

Under conditions where eq 2.9 holds, the thickness grows linearly in time, $R/R_e \cong t/\theta + e$, which is much more rapid than the logarithmic law governing Γ, in qualitative agreement with ellipsometric experiments.[7]

3. Quartz Crystal Microbalance

The quartz crystal microbalance (QCM) is a very sensitive tool used often to monitor the thickness of loss-free thin films deposited onto a flat surface from vacuum or vapor environments. Successes in maintaining stable vibration of quartz resonators in contact with liquids[18-23] and in modeling the quartz resonator response in lossy media[24,25] open a spectrum of new applications for this device.

3.1. Operating Principle of the QCM. The QCM's operating principle resembles that of surface loading rheological instruments used to measure high-frequency linear viscoelastic properties of polymeric liquids. Quartz is piezoelectric; thus when a periodic voltage is applied across electrodes affixed to the surfaces of a thin quartz plate, it vibrates at the excitation frequency. On the basis of this, a quartz crystal "resonator" can be built: By placing an appropriately cut quartz plate, equipped with surface electrodes, into the feedback network of an oscillator circuit, the circuit/crystal assembly can be made to oscillate indefinitely at or near one of the system's resonance frequencies. Given a properly designed plate, electrodes, and circuit, the plate can serve as a probe of physical phenomena occurring on the electrode's surface, since the resonator's operating point is very sensitive to the interaction between the plate and its environment. The main practical difficulty for applications in liquid media is maintaining stable vibration of the quartz plate, which is usually difficult due to the liquid's strong damping effect.

By analogy with the analysis of surface loading rheological devices, it is possible in principle to deduce a liquid's physical properties (density, linear viscoelastic properties) in a region near the quartz plate from measured shifts in

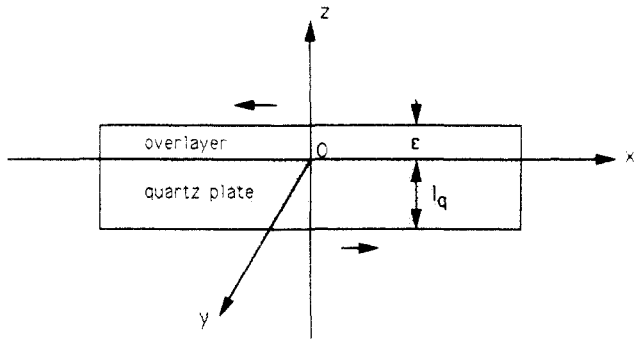

Figure 1. Schematic of a one-dimensional, composite resonator. Arrows along the x axis indicate the shear-thickness mode of deflection.

the circuit's operating point upon contact with the liquid (i.e. from shifts in the resonator's operating frequency and (complex) impedance). In the majority of applications published to date, including the present work, only frequency shifts are measured, which does not permit a direct evaluation of the liquid's properties. However, Kanazawa and co-workers[24,25] proposed a mechanical model for QCM frequency shifts which can be applied to a variety of situations, including lossy media, and which has clear physical interpretations. The theory identifies the QCM operating frequency, f, with the mechanical resonance determined by finding the lowest eigenfrequency of a shear wave propagating normal to the plate. Although the theory is purely mechanical, it correctly predicts experimental frequency shifts to within a numerical prefactor for two well-studied cases: a thin elastic overlayer and a viscous liquid reservoir. We use this approach as the basis of our analysis of QCM frequency shifts during polymer adsorption.

3.2. Kanazawa's Model for the QCM Response. Figure 1 shows the quartz crystal–overlayer system schematically. The thickness of the quartz crystal is l_q and that of the overlayer is ϵ. The coated quartz plate vibrates in the shear-thickness mode with a shear strain along the x direction, as indicated in Figure 1. One determines the mechanical resonance by finding the steady-periodic solution to the equations of motion permitting propagation of a shear wave through both the quartz and the overlayer. This solution must match at the interface both the shear displacement and shear stress and imply stress-free surfaces. The boundary conditions define a lowest eigenfrequency for a steady-periodic motion. Comparison with the corresponding frequency for an unloaded crystal defines the frequency shift due to the addition of the overlayer. Kanazawa solved this problem for a linear Voigt–Kelvin overlayer.

For an unloaded crystal ($\epsilon = 0$), one finds the resonance frequency, f_o

$$f_o = (1/2l_q)(\mu_q/\rho_q)^{1/2} \tag{3.1}$$

where μ_q and ρ_q are the shear modulus and mass density of quartz, respectively. Two limits of Kanazawa's result for the Voigt–Kelvin overlayer are of particular interest, one for thin elastic overlayers and the other for infinite viscous reservoirs. One obtains the elastic limit by first letting the viscosity of the overlayer, η_o, approach zero with all other physical constants fixed. When, in addition to $\eta_o \to 0$, the overlayer is thin enough that $\omega\epsilon(\rho_o/\mu_o)^{1/2} \ll 1$, where μ_o and ρ_o are the overlayer's shear modulus and density, one gets

$$\tan(\pi\Delta\omega/\omega_o) = -\omega\rho_o\epsilon/(\rho_q\mu_q)^{1/2} \tag{3.2}$$

where ω is the angular frequency of the loaded resonator and $\Delta\omega \equiv \omega - \omega_o = 2\pi(f - f_o)$ is the angular frequency shift due to loading. If the frequency shift is small enough that $\Delta\omega/\omega_o \ll 1$ then Sauerbrey's equation[26] is obtained from eq 3.2

$$\Delta f = -2f_o^2\rho_o\epsilon/(\rho_q\mu_q)^{1/2} \tag{3.3}$$

Equation 3.3 has been verified experimentally, to within a numerical prefactor, for elastic overlayers with $\rho_o\epsilon/\rho_q\mu_q$ up to about 0.02.[27,28]

Purely viscous overlayers correspond to the limit $\mu_o \to 0$ with all other physical constants fixed. For contact with a semiinfinite viscous reservoir one also takes $\epsilon \to \infty$. In this case, the predicted frequency change reduces to

$$\tan(\pi\Delta\omega/\omega_o) = -\omega\rho_o(\eta_o/2\omega\rho_o)^{1/2}/(\rho_q\mu_q)^{1/2} = -(\omega/(2\rho_q\mu_q))^{1/2}(\rho_o\eta_o)^{1/2} \tag{3.4}$$

By comparing with eq 3.2, one can interpret that the frequency shift caused by the contact with a viscous liquid bath results from loading by the mass of liquid within a decay length of $d(\omega) = (\eta_o/2\omega\rho_o)^{1/2}$ (typically $\sim O$ (1000 Å) for common liquids).

When, in addition to $\mu_o \to 0$ and $\epsilon \to \infty$, $\Delta\omega/\omega_o \ll 1$, eq 3.4 reduces to

$$\Delta f = -(f_o^{3/2}/(\pi\rho_q\mu_q)^{1/2})(\rho_o\eta_o)^{1/2} \tag{3.5}$$

Bruckenstein[20] arrived at this result by dimensional analysis; of course, his formula differs by a numerical prefactor. The relationship $\Delta f \sim (\rho_o\eta_o)^{1/2}$ predicted by eq 3.5 has been verified for a number of low molecular weight liquids with viscosities on the order of centipoise.[20-23].

Two additional results from Kanazawa's theory are relevant to subsequent discussion. If one takes the limit $\epsilon \to \infty$ in Kanazawa's general result for the Voigt–Kelvin overlayer, the prediction is in the form

$$\tan(\pi\Delta\omega/\omega_o) = -\omega\rho_o d(\omega)/(\rho_q\mu_q)^{1/2} \tag{3.6}$$

where $d(\omega)$ is a decay length which is always smaller than that for the corresponding viscous fluid (i.e. a Newtonian fluid with density ρ_o and viscosity η_o). For example, in the limit $\eta_o\omega/\mu_o \gg 1$ we find $d \simeq (\eta_o/2\omega\rho_o)^{1/2}[1 - (\eta_o\omega/\mu_o)^{-1} + O((\eta_o\omega/\mu_o)^{-2})]$ while for $\eta_o\omega/\mu_o \ll 1$, $d \simeq (\eta_o/2\omega\rho_o)^{1/2}(\eta_o\omega/2\mu_o)^{1/2}[1 + O(\eta_o\omega/\mu_o)]$. Hence, Kanazawa's theory predicts smaller frequency shifts from loading with a viscoelastic reservoir than from a purely viscous media with the same density and viscosity.

Finally, for the limiting cases of a thin elastic overlayer and of an infinite reservoir, realistic values of the physical constants for typical systems indicate $\Delta\omega/\omega_o \ll 1$ in either limit. This permits derivation of an additivity principle: the net frequency shift due to the combined loading by a thin elastic overlayer and an infinite reservoir in series is the sum of each effect in isolation (Appendix A). Kanazawa et al.[22] have verified this additivity by experiment for viscous fluid reservoirs.

3.3. QCM Response during Polymer Adsorption. We give here a preliminary analysis of QCM frequency shifts during polymer adsorption, based on Kanazawa's results. When the QCM contacts a dilute polymer solution, one measures the total frequency change Δf relative to the resonator frequency with the crystal in contact with air. This includes a frequency shift caused by the adsorbed layer and a shift due to the dilute homogeneous solution adjacent to the adsorbed layer. Comparing the order of magnitude estimates of the shear relaxation time for the semidilute adsorbed layer, τ_{se}, with the oscillation period of the quartz crystal, τ_q, shows clearly that the adsorbed

layer should behave like a thin elastic overlayer since $\tau_q \ll \tau_{se}$ (Appendix B). Comparing the relaxation time of a dilute solution of polystyrene (PS) with a molecular weight $M = 400\,000$ with τ_q shows that the two are comparable, implying that the bulk solution should affect the frequency like a linear viscoelastic reservoir.

From the additivity principle developed in Appendix A, we expect that the total frequency shift Δf is the sum of the frequency change caused by the elastic, adsorbed layer alone, Δf_μ, plus the shift caused by the dilute, homogeneous reservoir alone, Δf_η:

$$\Delta f = \Delta f_\mu + \Delta f_\eta \tag{3.7}$$

Accordingly, Δf_η should occur immediately upon contact between the crystal and the polymer solution; it characterizes the bulk solution properties. The remaining part, Δf_μ, should develop with time as the adsorption process proceeds.

One can estimate the frequency shift due to the adsorbed layer from Sauerbrey's law (eq 3.3):

$$\Delta f_\mu \simeq -2f_o^2 \rho R/(\rho_q \mu_q)^{1/2} \tag{3.8}$$

Where ρR is the areal mass density of the adsorbed layer, $\rho R = \int_0^R \rho(z)\,dz$, with $\rho(z)$ being the local mass density in the adsorbed layer. R is the effective depth defined by $\tau_q = \tau_{se}(c(R,t))$; i.e. R is defined by the depth of the mixture coupled elastically to the crystal. Of course, we do not expect that eq 3.8 gives the correct numerical prefactor, but this relation should be correct in predicting $\Delta f_\mu \sim \rho R$.

Neglecting the volume change on mixing and carrying out the integration of $\rho(z)$ gives

$$\rho R = \rho_1 R + m\delta\Gamma \tag{3.9}$$

where ρ_1 is the pure solvent mass density, m is the monomer mass, and $\delta = (\hat{v}_1 - \hat{v}_2)/(\hat{v}_1)$ with $\hat{v}_i$ being the partial specific volume of component i ($i = 1$ means solvent while $i = 2$ means polymer).

This analysis predicts that through Δf_μ, the QCM detects a linear combination of the solvent areal density trapped in the adsorbed layer and the adsorbed chain areal density. From ellipsometric results,[7a] which show that during homopolymer adsorption R develops much more quickly than does Γ, we anticipate that the first term on the right in eq 3.9 dominates on relatively short times scales, while the second term will dominate on long time scales. From eq 2.9, one expects for the mass coverage $A \equiv m\delta\Gamma = K \ln(t/\Theta + e) + K'$ with $K = m\delta/a^2$ and $K' = m\delta\Gamma_e$. Since we expect $e \ll 1$ one gets on time scales $t \sim O(\theta)$

$$A \cong 2.303K \log t + K' - 2.303K \log \theta; \quad t/\theta \sim O(1) \tag{3.10}$$

as a simple law expected for an entry-controlled adsorption process.

4. Experimental Section

4.1. Experimental Apparatus. A schematic of our QCM apparatus appears in Figure 2. A thermostated air bath (A), equipped with a heat source (B), a temperature controller (C) (Yellow Springs Instruments Model 63 RC, nominal accuracy ±0.05 °C), a thermocouple (D), a thermometer (E), and a circulation fan (F), houses the QCM. The QCM consists of an oscillator circuit (G) powered by a dc power supply (H) (Hewlett Packard, 6214B, 0–10 V) and a sample cell (I). The circuit frequency is measured by a digital frequency counter (J) (Philips, Model PM6673), and acquired by a IBM PC AT (K) equipped with a digital data acquisition board (Metrabyte, Model MBC-488).

There is no standard circuitry available for QCM applications in lossy media; several different designs have been published.[19-21]

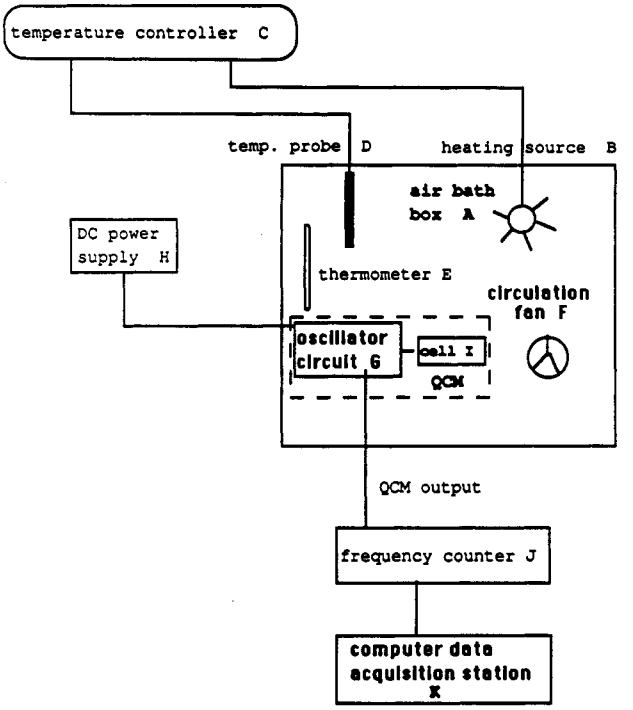

Figure 2. Schematic of a QCM apparatus.

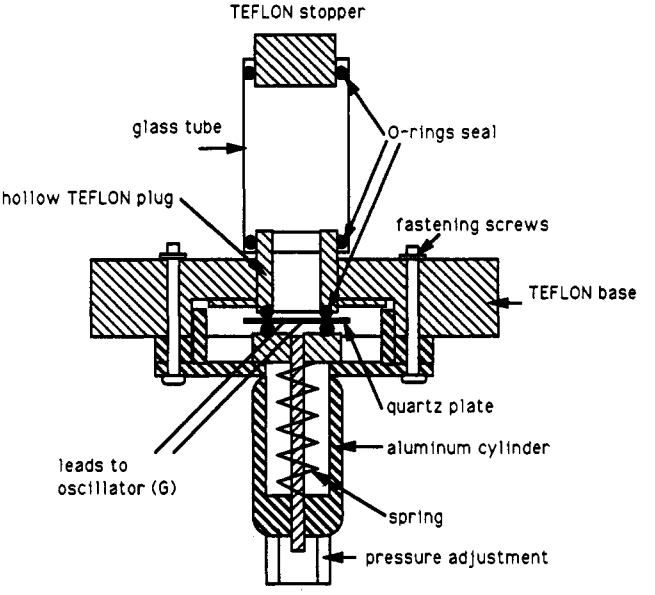

Figure 3. Schematic of the sample cell.

On the basis of these, we designed a driving circuit consisting of an oscillating stage, an amplifier-buffer stage, voltage stabilizers, and high and low frequency interference filters. The oscillating stage is similar to that of Weil et al.[21]

A schematic of our sample cell appears in Figure 3. It consists of a glass liquid container sealed by a Teflon stopper, a Teflon base, and a spring-loaded piston which gently presses the quartz plate upward between opposing O-rings to prevent liquid leakage. The quartz crystals we used were AT-cut, 0.55 in. in diameter and 0.007 in. in thickness with a nominal operating frequency of either 5.0 or 10.0 MHz (International Crystal Manufacturing Co. Inc., Oklahoma City). According to the manufacturer, the electrodes are gold, approximately 1000 Å thick and 0.205 in. in diameter. The temperature sensitivity of the crystals, as stated by the manufacturer, is $\Delta f/f_o \simeq 5$ ppm within the range −10 to +60 °C, which means the effect of temperature fluctuations in our thermostat can be neglected. The sample cell proved effective both in sealing and in preventing liquid evaporation. It was found that the mounted quartz plates oscillated stably in air at a frequency roughly 1 MHz less than the nominal value.

4.2. Preliminary Experiments. Preliminary experiments were carried out to test the stability and response to viscous

Table I. Adsorption Experiments for PS onto Gold from Cyclohexane at 34.5 °C

series	run no.	$10^{-6} M_w$	M_w/M_n	c_b (g/dL)	c_b/c^*	ρ^b (g/cm^3)	$\eta - \eta_s$[c,d] (cP)
A	A1	3[a]	1.2	0.592	1/6	0.780	0.802
	A2	1.8	1.15	0.8	1/6	0.781	0.842
	A3	1.03[a]	1.06	1.0	1/6	0.781	0.792
	A4	0.9	1.10	1.14	1/5.7	0.781	0.732
	A5	0.4	1.06	1.6	1/6	0.783	0.792
	A6	0.2077[a]	1.05	2.5	1/6	0.785	0.912
B	B7 (=A5)	0.4	1.06	1.6	1/6	0.783	0.792
	B8	0.4	1.06	0.243	1/40	0.779	0.092
	B9	0.4	1.06	0.05	1/200	0.779	0.019
	B10	0.4	1.06	0.0243	1/400	0.779	0.009
	B11	0.4	1.06	0.00243	1/4000	0.779	0.001

[a] Obtained from Polysciences Inc.; remaining samples from Pressure Chemical Co. [b] Solution density $\rho = \rho_1 + c_b(1 - \rho_1/\rho_2)$, where the pure cyclohexane density $\rho_1 = 0.7785$ g/cm^3 [31a] and the pure PS density $\rho_2 = 1.065$ g/cm^3.[31b] [c] Pure cyclohexane viscosity $\eta_s = 0.758$ cP.[30] [d] Solution viscosity $\eta = \eta_s\{1 + c_b[\eta] + 0.375[\eta]^2 c_b^2\}$ with the intrinsic viscosity $[\eta] = 8.2 \times 10^{-2} M_w^{1/2}$.[31,32]

media of our QCM. To begin a typical experiment, all parts of the sample cell were cleaned as follows. First, the parts are immersed in warm (~50 °C) toluene (two immersions, about 1 h each) and then rinsed thoroughly with ethanol at room temperature. Then, each part is gently scrubbed with a sterile cotton swab saturated with cyclohexane, and finally immersed in warm cyclohexane for about 1 h. After the sample cell is assembled, it is dried under vacuum at room temperature and then placed into the thermally controlled air bath. Prior to the beginning of the measurements, the liquid sample, the circuit, and the sample cell are allowed to equilibrate thermally (~3 h) in the air bath. The data acquisition is then triggered via an interfacing program in the PC. The data collection rate is 1 Hz; data collected within the specified time interval are averaged to produce one entry stored in an ASCII file for later analysis. For the preliminary tests described below, the time interval for averaging was 1 min.

Polymer adsorption is a relatively slow process and requires a long time scale to reach equilibrium (~O (10 h) for the systems investigated in this work[7,10]). Therefore, it was crucial to minimize long time-scale frequency drift caused by factors other than adsorption. We therefore tested the stability of the QCM in contact with pure cyclohexane over extended time periods. Such tests gave an average drift rate of 3 Hz/day. This level is small enough compared to frequency changes due to polymer adsorption to be neglected with confidence.

To check for the proper response to a viscous liquid reservoir, we measured the frequency shifts relative to air for contact with liquid cyclohexane at temperatures between 30 and 38 °C and therefore at different cyclohexane viscosities and compared the measured shifts with eq 3.5. For this comparison ρ_q and μ_q were taken as 2.648 g/cm^3 and 2.947×10^{11} dynes/cm^2, respectively.[22] The change in density with temperature for liquid cyclohexane from 30 to 38 °C was ignored, and a constant value of 0.7785 g/cm^3 was used.[31] A temperature-dependent viscosity η was calculated from $\eta = 6.1739 \times 10^{-5} \exp(1481.6/T)$ where T is in Kelvin and η is in poise.[30] The comparison verified $\Delta f \sim \eta^{1/2}$, as expected, but gave a numerical prefactor about 10 times that shown in eq 3.5. (Recall that eq 3.5 is based on a purely mechanical model, so a discrepancy in the prefactor is expected.) In what follows, this experimentally determined prefactor was used for all conversions between frequency shifts and adsorbed layer characteristics.

4.3. Adsorption Experiments. Nearly monodisperse polystyrene (PS) was obtained from Polysciences Inc. (Warrington, PA) and Pressure Chemical Co. (Pittsburgh, PA). The molecular weights and polydispersity indices of the polymers as specified by the manufacturers are given in Table I. HPLC grade cyclohexane was obtained from Aldrich Chemical Co., Inc. (Milwaukee, WI). All materials were used as received.

PS solutions were prepared by slow stirring of the as-received powder in an appropriate volume of cyclohexane on a hot plate at about 60 ± 10 °C for about 5 h. The resulting clear solutions were stored in sealed glass bottles placed in the thermostated air bath at 34.5 °C until ready for use.

Each adsorption experiment was carried out as follows. After the crystal was mounted, its frequencies in contact with air and with pure liquid cyclohexane were measured for an extended time to ensure a stable base line. To monitor adsorption, the pure cyclohexane was withdrawn and replaced with the thermostated PS solution using a Teflon syringe. The frequency was then monitored continuously by the data acquisition system until a new stable base line was achieved.

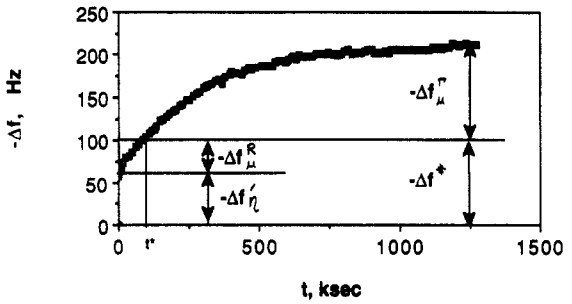

Figure 4. Frequency shift versus time during run A5 of Table I. The characteristic shifts discussed in the text are indicated.

Table I summarizes the experiments done. These were designed to probe the effects of both polymer molecular weight (series A) and of bulk polymer concentration (series B). Table I also gives the weight average molecular weight, M_w, polydispersity, M_w/M_n, bulk solution concentration, c_b, the (calculated) ratio c_b/c^*, the (calculated) bulk solution density, ρ, and the (calculated) difference between the bulk solution viscosity η and solvent viscosity η_s.

For series A, c_b was selected to be in the dilute regime ($\simeq c^*/6$) but above the saturation concentration c_{sat} for the adsorption isotherm, as determined in the study by Takahashi et al.[7a] For series B, the polymer molecular weight was kept fixed at 400 000 and five values of c_b were used from above c_{sat} (for M = 400 000, $c_{sat} \simeq 0.243$ g/dL[7a]) to well below c_{sat}. The temperature of the QCM apparatus was carefully controlled by an air thermostat at the Θ temperature for PS–cyclohexane (34.5 °C). For the data averaging, a 2-min time averaging interval was used in runs A2, A3, A5, and A6 and a 5-min interval was used in the remaining runs.

5. Experimental Results and Discussion

A typical display of the frequency change during adsorption relative to the frequency measured in pure cyclohexane appears in Figure 4 (run A5 in Table I). The frequency clearly decays monotonically over a long time scale (~O (10^3 ks) for complete equilibrium) indicating a deposition phenomena. The reproducibility of such kinetic measurements was checked by repeated measurements for PS with M_w = 1 030 000. The reproducibility is fairly good, at about ±10%.

To analyze data such as in Figure 4 for $\Gamma(t)$, we applied two separate protocols. The instantaneous frequency drop in the real time kinetic plots like Figure 4 is attributed to the damping from contact of the crystal with the homogeneous bulk PS solution, i.e. the term Δf_η discussed earlier. Of course, only the portion of this shift, $-\Delta f'_\eta$, relative to

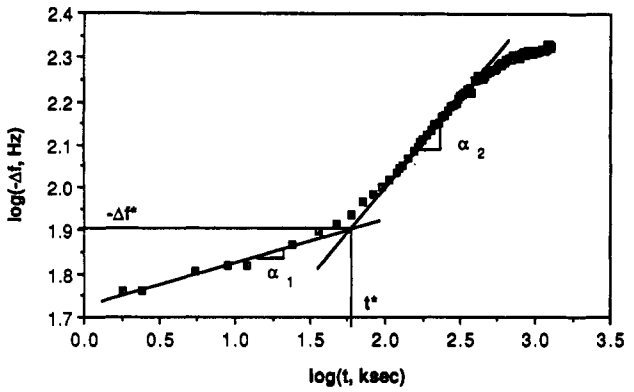

Figure 5. Log–log plot of the frequency shift versus time for run A5 in Table I.

that induced by pure cyclohexane is seen, as illustrated in Figure 4. After this instantaneous shift, the adsorbed layer begins to develop and the term Δf_μ contributes. This term has two parts (see eqs 3.8 and 3.9), one associated with the development of the layer's thickness R and the second associated with development of the coverage Γ. In one procedure, we separated these empirically, employing log–log plots. Figure 5 shows a replot of Figure 4 in log–log format. The data clearly show two linear portions, and this was true in all the experiments we ran (similar results were found by Granick et al.[9] for the system poly(methyl methacrylate)–carbon tetrachloride–Ge/Ar/Se alloy at 25 °C). The intersection of the two linear parts gives a characteristic time t^* and a characteristic frequency change Δf^*. From eq 3.9, Δf_μ ($=\Delta f - \Delta f'_\eta$) corresponds to $\Delta f_\mu^R + \Delta f_\mu^\Gamma$ where $\Delta f_\mu^R \simeq -2f_o^2\rho_1 R/(\rho_q\mu_q)^{1/2}$ and $\Delta f_\mu^\Gamma \simeq -2f_o^2 m\delta\Gamma/(\rho_q\mu_q)^{1/2}$. Recall that Δf_μ^R should evolve much faster than Δf_μ^Γ and should dominate Δf_μ at relatively short times. So, in one treatment of the data we assigned

$$|\Delta f_\mu^\Gamma| = |\Delta f_\mu| - |\Delta f_\mu^R| = |\Delta f| - |\Delta f^*| \tag{5.1}$$

and evaluated the mass coverage, $A(=m\delta\Gamma)$, by

$$A = -\alpha\Delta f_\mu^\Gamma(\rho_q\mu_q)^{1/2}/(2f_o^2) \tag{5.2}$$

where α is a numerical prefactor determined experimentally, as described in section 4.2.

To check that this interpretation is reasonable, we compared typical equilibrium values from our measurements of $|\Delta f_R^\mu| = |\Delta f^*| - |\Delta f'_\eta|$ and $|\Delta f_\mu^\Gamma| = |\Delta f(t \to \infty)| - |\Delta f^*|$ with those expected from ellipsometric data.[7a] The ellipsometric data give for PS with $M_w = 400\,000$, $R_e \cong 300$ Å and $A \cong 5 \times 10^{-7}$ g/cm^2. The corresponding frequency change $\Delta f_\mu = \Delta f_\mu^R + \Delta f_\mu^\Gamma$ is, according to eqs 3.8 and 3.9 including the appropriate prefactor, −160 Hz, in good agreement with our measured value of $\Delta f_\mu = \Delta f - \Delta f'_\eta = -150$ Hz. However, according to the ellipsometric data, $\Delta f_\mu^R \cong -130$ Hz and $\Delta f_\mu^\Gamma \cong -30$ Hz, while our experimental values for $M_w = 400\,000$ show $|\Delta f_\mu^\Gamma|$ to be larger than $|\Delta f_\mu^R|$ (100 vs 50 Hz). These results are typical of all experiments. There are several possible explanations for this discrepancy, including that the empirical procedure for splitting Δf_μ^R and Δf_μ is inaccurate.

As an alternate treatment of the data, we simply ignored the first term on the right-hand side of eq 3.9 and treated the frequency shift $\Delta f - \Delta f'_\eta$ as due to the coverage only. This alternate treatment of the data did not lead to significantly different final conclusions from those reached using the first protocol, and so the results of this second method of data treatment are omitted in what follows.

5.1. Instantaneous Frequency Shifts. Assuming the PS bulk solutions in Table I are linearly viscous, one can use eq 3.5 (with an experimentally determined prefactor) to predict the instantaneous frequency shift, $\Delta f_\eta = \Delta f'_\eta + \Delta f_s$, where Δf_s is the shift induced by pure solvent. The measured and computed values of Δf_η are listed in Table II. The measured values are consistently smaller than those predicted, although for series B at the lowest values of c_b (runs B8–B11) the agreement is reasonable. A plausible explanation for this systematic discrepancy is that the bulk solutions behave viscoelastically, which is supported by the estimates of shear relaxation times (Appendix B). For these conditions, the instantaneous frequency shifts should be compared to a model for the effect of a homogeneous, linear viscoelastic reservoir rather than for a viscous reservoir. Eq 3.6, derived for a Voigt–Kelvin reservoir, predicts a frequency shift smaller than that for a viscous reservoir, in qualitative agreement with the experiments. A more detailed comparison between data and a model for the QCM response in contact with a viscoelastic liquid reservoir is in progress.

Table II. Experimental and Calculated Instantaneous Frequency Shifts from Bulk Polymer Solutions

run no.	exp $-\Delta f'_\eta$ (Hz)	exp $-\Delta f_\eta = -\Delta f'_\eta - \Delta f_s$ (Hz)	predicted[a] $-\Delta f_\eta$ (Hz)	ratio experimental/ predicted
A1	37	1600 ± 10	2787	0.57
A2	19	1590 ± 20	2825	0.56
A3	56	1840 ± 20	2780	0.66
A4	53	1680 ± 20	2726	0.62
A5	84	1725 ± 5	2784	0.62
A6	112	1760 ± 5	2894	0.61
B7	84	1725 ± 5	2784	0.62
B8	29	1780 ± 5	2062	0.86
B9	43	1580 ± 5	1965	0.80
B10	41	1580 ± 10	1952	0.81
B11	68	1600 ± 10	1942	0.82

[a] Calculated using eq 3.5 with an experimentally determined numerical prefactor.

5.2. Effect of Polymer Molecular Weight. We now analyze the effect of molecular weight on $A(t)$ based on the rate equations, eq 2.5 and its integrated form, eq 3.10. To recast the former in terms of A, we multiply by $m\delta$ and introduce the definition $A \equiv m\delta\Gamma$ to get

$$dA/dt = K_{si}^o(A)\rho_b \tag{5.3}$$

where $K_{si}^o(A) = \delta K_{si}(A)$ and $\rho_b = mc_b$ means the bulk polymer mass concentration. Eqs 2.6 and 2.7 predict $K_{si}^o \sim N^{-5/2}/\ln N$, indicating that K_{si}^o should decay strongly with molecular weight. Order of magnitude estimates of K_{si}^o for $M_w = 400\,000$ suggest the range of values $10^{-8} < K_{si}^o < 10^{-5}$ (K_{si}^o in cm/s) for entry-controlled adsorption by the end-in reptation mechanism (Appendix C).

To study the coverage dependence of K_{si}^o by eq 5.3, we first extracted Δf_μ^Γ for runs A1–A6 by the first protocol discussed above, and plotted A ($= -\alpha\Delta f_\mu^\Gamma(\rho_q\mu_q)^{1/2}/2f_o^2$) versus t. We then curve fit the measured $A(t)$ for each of the runs A1–A6 to find smooth polynomial representations of $A(t)$. These allowed preparation of plots of $K_{si}^o(A)$ vs A. Figure 6 shows the results; K_{si}^o decreases with A, as expected intuitively since greater coverage should retard the entry process. However, the predicted molecular weight dependence is not seen. Also, the magnitude of the K_{si}^o found is 2–5 orders smaller than that expected on the basis of entry-controlled adsorption governed by end-in reptation. In order to match the measured and predicted magnitudes while the adsorbed layer depth is fixed at a realistic value, an unrealistically low diffusion coefficient

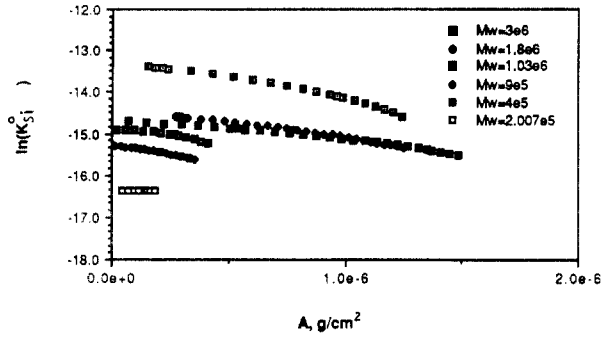

Figure 6. Log of the transmission coefficient K_{sj}° (cm/s) versus the mass absorbance A (g/cm^2) for runs A1–A6 in Table I.

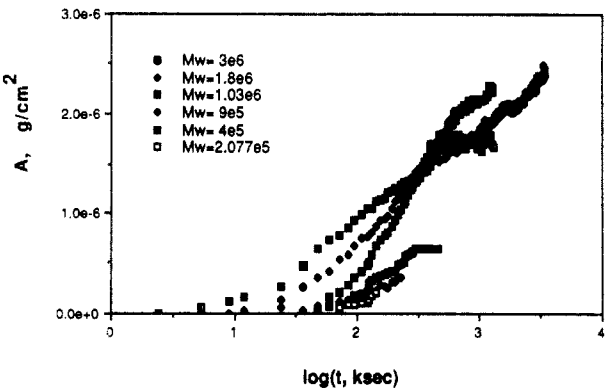

Figure 7. Mass absorbance A (g/cm^2) versus log t (ks) for runs A1–A6 in Table I.

($D \sim O(10^{-17}$ cm^2/s)) must be used in the theory. Clearly, there is a significant discrepancy between the theory and experiment. The same conclusion is also reached if one applies eq 3.10 to the data.

This was done by plotting A versus log t. Figure 7 shows the results; for each run the data show a linear portion when plotted in semilog format, as expected. Values of K were measured from the slope of least-squares fits to the linear portions; values of t_{int} were determined from the least-squares intercepts of the linear portions with the log t abscissa. These are collected in Table III. Recall that eq 3.10 predicts K independent of N. Also, since in runs A1–A6 c_b was deliberately chosen to be $c^*/6$ in order to remain in the plateau regime of the adsorption isotherm, t_{int} is predicted to be proportional to $N^3/\ln N$ for this series of experiments.

First consider the magnitude of the values found for K and t_{int} in comparison with order of magnitude estimates for K and t_{int} from theory. Table III gives the values expected for K, t_{int}, and θ/θ_6 ($=t_{int}/t_{int,6}$). The experimental values of K have the expected magnitude and are independent of molecular weight, in agreement with the prediction. However, the experimental values of t_{int} are much larger than predicted, indicating an unexpectedly slow process; an unrealistically low diffusion coefficient ($D \sim O(10^{-17}$ cm^2/s)) is needed to match theory and experimental results for t_{int} in order of magnitude if one fixes the adsorbed layer depth at a realistic value, in agreement with the foregoing analysis of the transmission coefficients. Also, the experimental values of t_{int} do not show a systematic variation with molecular weight, whereas the theory predicts $t_{int} \sim N^3/\ln N$. There are several plausible explanations for these discrepancies.

One possibility is that the assumption of control by entry in the theory is erroneous. Since PS has a high glass transition temperature ($\simeq$100 °C), it is possible that a glasslike layer develops very near the adsorbing wall. If this is so, the wall friction would be very large, slowing down the spreading process. Then spreading rather than entry might limit the incorporation of chains into the adsorbed layer, giving a somewhat different (slower) kinetic law for $\Gamma(t)$ than eq 2.9. It should be noted however that spreading control, according to deGennes,[6] would still involve a strong molecular weight dependence due to the reptation mechanism, and this is not seen in the data.

A mechanism which may participate and possibly dominate in the formation of the adsorbed layer, and which is neglected in refs 5 and 6, is osmotic compression or mutual diffusion, which has a much weaker molecular weight dependence than the reptative self-diffusion process assumed in section 2. One would guess this mechanism is very fast relative to reptation of incoming chains into the layer and therefore too fast to explain the long time scales involved. However, osmotic compression could be greatly slowed if the region near the wall approaches melt densities and slow, glasslike relaxations impede the process.[34] This mechanism could account for both the long time scale and lack of molecular weight dependence.

Another possibility is that both the long time scale observed and the lack of molecular weight dependence in the characteristic times are due to polydispersity in our samples.[35] The rationale for this is as follows. The limited kinetic data published for PS adsorption onto metals (e.g. refs 7 and 10) do suggest that polydisperse samples have a longer time scale for adsorption than the corresponding monodisperse material. Studies of adsorption exchange kinetics[36] suggest a reason for this: During the adsorption of polydisperse material, low molecular weight species deposit first and are later displaced by higher molecular weight chains in a slow exchange process. While this scenario could explain the long time scales seen in our experiments relative to other reports of adsorption kinetics in similar systems (e.g. refs 7 and 37), it does not explain in any obvious way the lack of (average) molecular weight dependence we find in the characteristic times for adsorption.

5.3. Effect of Bulk Polymer Concentration. The runs in series B of Table I probe the effect of bulk concentration c_b on the kinetics for c_b from above the value of c_{sat} reported by Takahashi et al.[7] to well below it. The kinetics of the mass coverage A for runs B7–B11 appear

Table III. Experimental and Predicted Values of the Parameters K, t_{int}, and θ

		10^7K (g/cm^2)			t_{int} (ks)			θ/θ_6[c]	
run no.	$10^{-6}M_w$	exp	r^2 [a]	theor[b]	exp	r^2	theory	exp	theor
A1	3.0	5	0.99	1.5	20	0.99	32	0.3	3204
A2	1.8	2	0.98	1.5	30	0.98	7	0.5	698
A3	1.03	4	0.97	1.5	60	0.97	1.4	1.0	140
A4	0.9	6	0.99	1.5	30	0.99	1.0	0.5	99
A5	0.4	8	0.99	1.5	50	0.99	0.08	0.8	8
A6	0.2077	2	0.90	1.5	60	0.9	0.01	1	1

[a] r^2 means the correlation coefficient in linear regression fitting. [b] Theoretical values of K, t_{int}, and θ were evaluated using the method in Appendix D, where an example calculation for run A5 is given. [c] Subscript 6 denotes the value for run A6.

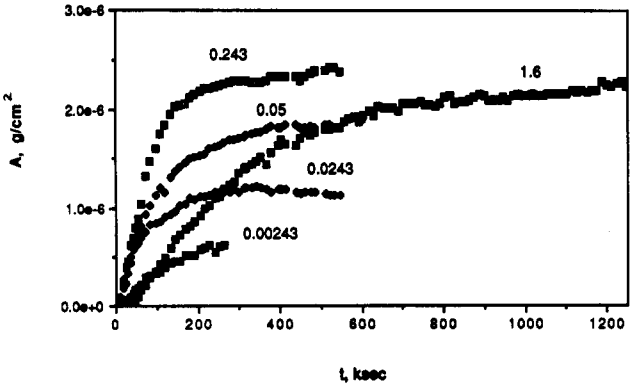

Figure 8. Mass absorbance A (g/cm^2) versus time t (ks) for runs B7–B11 in Table I. The parameter shown indicates the bulk polymer concentration (g/dL).

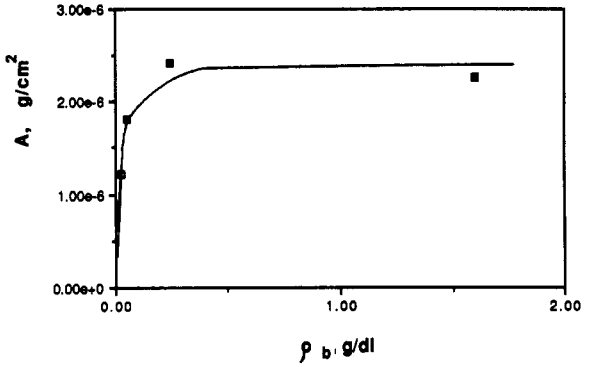

Figure 9. Adsorption isotherm derived from equilibrium frequency shifts in runs B7–B11 in Table I.

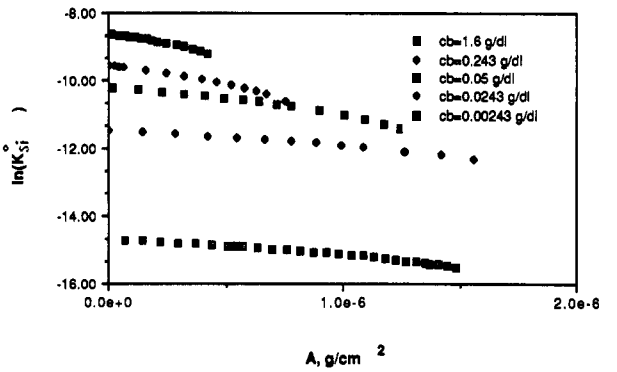

Figure 10. Log of the transmission coefficient K_{si}^{o} (cm/s) versus the mass absorbance A (g/cm^2) for runs B7–B11 in Table I.

in Figure 8. All plots show a long time scale ($\sim O$ (10^2 – 10^3 ks)) for the deposition of chains. The adsorption isotherm for PS with M_w = 400 000 can be obtained from the equilibrium values in Figure 8. The result is shown in Figure 9; the isotherm has the expected shape. This result lends confidence to the procedure for extracting Δf^{Γ} from Δf (see Figure 4).

Using the curve fitting procedure described in the previous section, we obtained $K_{si}^{o}(A)$ vs A for series B, as shown in Figure 10. Again, K_{si}^{o} decreases as A increases, as expected. However, a clear, systematic dependence on c_b is displayed, indicating that K_{si}^{o} is an apparent function of both A and c_b. Values of the transmission coefficient at half-saturation, $A = A_e/2$, are collected in Table IV. The apparent c_b dependence of K_{si}^{o} for $A = A_e/2$ can be represented empirically

$$K_{si}^{o} \sim c_b^{-(0.65\pm0.05)}; \quad c_b \le c_{sat}, A = A_e/2 \qquad (5.4)$$

Equation 5.4 expresses in compact form what is clearly shown in Figure 10: the higher is c_b, the smaller is K_{si}^{o}.

Table IV. Transmission Coefficients at Half-Saturation, K_{si}^{o}

run no.	c_b/c_{sat}[a]	K_{si}^{o}[b] (cm/ks)	$K_{si}^{o}/K_{si,11}^{o}$[c]
B7	6.6	2.45×10^{-7}	2×10^{-3}
B8	1.0	6×10^{-6}	0.05
B9	0.206	1.86×10^{-5}	0.15
B10	0.1	3.8×10^{-5}	0.3
B11	0.01	1.25×10^{-4}	1

[a] $c_{sat} \cong 0.243$ g/dL; estimated from ref 7a. [b] Measured from Figure 10. [c] Subscript denotes value for run B11.

This analysis shows that eq 2.5 is inadequate because it asserts that the transmission coefficient is a unique function of the coverage only. Figure 10 and eq 5.4 suggest that K_{si}^{o} depends on the history of the adsorbed layer's development. In particular, layers prepared under a large driving force (i.e. large c_b) are less transparent than layers prepared under a small driving force for the same total coverage. This finding strongly suggests that the assumption of adiabatic growth is violated.

6. Summary and Conclusions

In this work we applied the QCM to measure the adsorption kinetics of linear, flexible PS chains from dilute Θ solutions onto a flat gold surface and investigated systematically the influences of polymer molecular weight and of bulk polymer concentration. To motivate analysis of the data, we reviewed de Gennes' preliminary ideas on adsorption kinetics which give simple kinetic formulas for the adsorbed layer thickness R and coverage Γ under Θ conditions.

In the analysis of the influence of molecular weight (runs A1–A6), we applied the rate equation for mass coverage A to find transmission coefficients $K_{si}^{o}(A)$. These decrease with A which is qualitatively correct. However, the transmission coefficients do not show the molecular weight dependence predicted by the theory. Furthermore, they are smaller than any reasonable estimate based on the theory, by at least 2 orders of magnitude. For example, if a reasonable value of the adsorbed layer thickness is assumed, then an unreasonably small diffusion coefficient ($D \sim O$ (10^{-17} cm^2/s)) is needed to match the experiment and theory in order of magnitude. These results indicate that, in this system, the adsorption kinetics are much slower than if governed by end-in reptation and are insensitive to molecular weight. The same conclusions were drawn from an analysis based on eq 3.10. Plots of A vs log t gave slopes K of the correct order and independent of molecular weight, as predicted. However, the time abscissa intercepts t_{int} did not depend on molecular weight as expected and were much larger than predicted. In toto, the analyses of the influence of molecular weight on the kinetics does not support the assumption of kinetic control by end-in reptation leading to eq 2.9.

In a second series of experiments, we probe the effect of bulk polymer concentration. The adsorption isotherm obtained from the equilibrium frequency shifts in this series agrees qualitatively with that found by Takahashi et al.[7a] An analysis of the transmission coefficients for this series using eq 5.3 again showed that K_{si}^{o} decreases as A increases, which is expected. But, we also found an apparent dependence on c_b:K_{si}^{o} increases as c_b decreases. This is not consistent with eq 5.3, and shows that the properties of a partially formed adsorbed layer depend on how it is prepared. This is clearly inconsistent with the assumption of adiabatic growth.

The results from the QCM measurements indicate that the adsorption of PS from dilute Θ solutions onto a flat gold surface is a relatively slow process whose rate has little or no molecular weight dependence and that the permeability of a partially formed adsorbed layer depends on the history of formation. To correctly model the adsorption kinetics, one should consider the slow spreading process when the wall friction is high and/or a collective transport mechanism which has weak molecular weight dependence. In such an analysis, memory effects undoubtedly play a key role.

Acknowledgment. The authors thank Mr. T. Y. Zhang for assistance with the circuit design and acknowledge financial support for the instrument development effort from the Office of Naval Research (Grant No. N00014-86-K-0642) and the National Science Foundation (Grant No. CTS-89-19665). T.Z.F. acknowledges support under a Boris Bakhmeteff Fluid Mechanics Fellowship (Columbia University).

Appendix A

Here we justify an additivity principle. Equations 3.2, 3.4, and 3.6 are in the form

$$\tan(\pi\Delta\omega/\omega_o) = D_i \tag{A.1}$$

where D_i is a dimensionless group. The subscript i denotes the limiting cases: $i = 1$ means the thin elastic overlayer while $i = 2$ means the infinite reservoir. These groups are

$$D_1 = -\omega\rho_o\epsilon/(\rho_q\mu_q)^{1/2} \tag{A.2a}$$

$$D_2 = -\omega\rho_o d(\omega)/(\rho_q\mu_q)^{1/2} \tag{A.2b}$$

For typical systems one finds $D_i \ll 1$ which permits linearization in $\Delta\omega/\omega_o$ to find eqs 3.3 and 3.5 and a similar analog for eq 3.6.

Now, for a crystal loaded with both a thin elastic overlayer and a reservoir in series, we find a condition of the form

$$\tan(\pi\Delta\omega/\omega_o) = g(D_1,D_2) \tag{A.3}$$

where g has the property

$$\lim_{D_i\to 0} g = D_j; \quad i = 1, 2, \quad i \neq j, \quad D_j \ll 1 \tag{A.4}$$

In a system where $D_i \ll 1$ for both $i = 1$ and $i = 2$ one can expand

$$g(D_1,D_2) \cong g_o + (\partial g/\partial D_1)_o D_1 + (\partial g/\partial D_2)_o D_2 + O(D_i^2) \tag{A.5}$$

where the subscript o means the value when $D_1 = D_2 = 0$. From eq A.4 we get $g_o = 0$, $(\partial g/\partial D_i)_o = 1$ and conclude

$$\tan(\pi\Delta\omega/\omega_o) \simeq D_1 + D_2 \quad \text{for} \quad D_i \ll 1 \tag{A.6}$$

Linearizing the left predicts additivity: The net frequency shift due to the combined loading by a thin elastic overlayer and a reservoir is the sum of frequency shifts due to each effect in isolation. This has been verified by experiment[22] for viscous fluid reservoirs.

Appendix B

Here, we estimate the shear relaxation times of a dilute solution of polystyrene (PS) at Θ conditions, τ_b, and of the adsorbed layer of PS on gold at Θ conditions, τ_{se}.

From Zimm,[29] the dominant relaxation time of an infinitely dilute polymer solution at Θ conditions is

$$T_{1\Theta} = 0.42M[\eta]\eta_s/(kTN_A) \tag{B.1}$$

where η_s is the solvent viscosity, T is the absolute temperature, $[\eta]$ is the intrinsic viscosity, M is the polymer molecular weight, k is Boltzmann's constant, and N_A is Avogadro's constant. For PS in cyclohexane at 34 °C, we have[30,31]

$$\eta_s = 6.1739 \times 10^{-5} \exp(1481.6/T) \text{ (poise)}$$

$$[\eta] = 8.8 \times 10^{-2} M^{1/2} \text{ (cm}^3\text{/g)} \tag{B.2}$$

As an approximation, $T_{1\Theta}$ can be used for τ_b. For M = 400 000, eq B.1 provides $T_{1\Theta} = 3 \times 10^{-6}$ s $\cong \tau_b$.

According to Adam and Delsanti[30] the dominant shear relaxation time $T_{R\Theta}$ at a finite polymer mass concentration, ρ_b, in the semidilute regime ($\rho_b/\rho_\Theta^* > 1$) can be expressed empirically

$$T_{R\Theta}/T_{1\Theta} \cong 10(\rho_b/\rho_\Theta^*)^{2.8}; \quad 1 < \rho_b/\rho_\Theta^* < 70 \tag{B.3}$$

where ρ_Θ^* is the overlap mass concentration given by $\rho_\Theta^* = M/(N_A R_F^3)$. Here $R_F = aN^{1/2}$ is the coil size in solution with a being the segment size. For polystyrene, $\rho_\Theta^* \simeq 61.5M^{-1/2}$ so that eq B.3 gives

$$\lim_{\rho_b\to\rho_\Theta^*} T_{R\Theta} \simeq T_{R\Theta}^* = 3 \times 10^{-5} \text{ s}$$

for PS with M = 400 000.

Now, according to de Gennes' description, the adsorbed layer possesses a self-similar structure out to a cutoff distance. Beyond this outer cutoff, the monomer density decays exponentially with distance from the wall. At equilibrium, the outer cutoff is R_F and the monomer density at that point is $\cong c^*$. For starved layers, the self-similar part is truncated at some depth $R < R_F$ and the corresponding monomer density is larger than c^*. Clearly then, $T_{R\Theta}^*$ is a reasonable lower bound estimate for τ_{se}.

Since the oscillation time for our QCM, $\tau_q = f_o^{-1} = 2 \times 10^{-7}$ s, we find $\tau_q \ll \tau_{se}$, meaning that the adsorbed layer responds elastically during oscillation. Since the τ_b is found to be the same order as τ_q, a bulk solution with M = 400 000 should behave viscoelastically. Actually, this will be true for PS molecular weights >100 000. For $M <$ 100 000, the bulk should behave more like a viscous reservoir.

Appendix C

Here we find an order of magnitude estimate for the transmission coefficient K_{si}^o for run A5. K_{si}^o is given by

$$K_{si}^o = \delta D/R \tag{C.1}$$

where $\delta = (\hat{v}_1 - \hat{v}_2)/\hat{v}_1$, with $\hat{v}_1$ and $\hat{v}_2$ being the specific volumes of solvent and polymer, respectively, and where R is governed by eq 2.7. Since $\hat{v}_1 = 1.285$ cm^3/g[31] and $\hat{v}_2 = 0.939$ cm^3/g,[31] one finds $\delta = 0.27$. For calculating R (see below) the segment size a is taken to be 2 Å.

The translational diffusion coefficient D for chain segments to cross the semidilute, adsorbed layer can be estimated from translational diffusion coefficients for bulk, semidilute solutions reported in ref 33. D should fall in the range $10^{-3} < DM^2\eta_s < 1$ for PS/cyclohexane solutions at 34.5 °C (Θ state), where D is in cm^2/s and the solvent viscosity η_s is in cP. For M = 400 000 and $\eta_s = 0.758$ cP,[30] we find $10^{-14} < D < 10^{-11}$; D is in cm^2/s for semidilute solutions.

For the order of magnitude estimate, we calculated K_{si}^o at half-saturation, i.e. at the mass coverage $A = A_e/2$, where A_e means the equilibrium mass coverage. In this case, eq 2.7 gives $R = R_e \exp(-\gamma_e/2)$. Since γ_e ($=a^2\Gamma_e$) was found to be $\cong 4$ (Appendix D) and $R_e = aN^{1/2}$ for Θ conditions, we find for M = 400 000 at half-saturation 10^{-8}

$< K_{si}^{o} < 10^{-5}$; K_{si}^{o} in cm/s is a realistic estimate based on the mechanism of end-in reptation.

Appendix D

Here we develop order of magnitude estimates of the parameters K, θ, and t_{int} for run A5. We evaluated these according to the following equations

$$K = m\delta/a^2 \tag{D.1}$$

$$\theta = R_e/(a^2 D c_b) \tag{D.2}$$

$$t_{int} = \theta e^{-\gamma_e} \tag{D.3}$$

where $\gamma_e = a^2\Gamma_e$.

For PS, $m = 2 \times 10^{-22}$ g, $a \cong 2$ Å, and $\delta = 0.27$ (see Appendix C), one finds $K \cong 1.5 \times 10^{-7}$ g/cm^2, independent of molecular weight.

For $M_w = 400\,000$, the translational diffusion coefficient D should fall in the range (see Appendix C) $10^{-14} < D < 10^{-11}$ (cm^2/s). Also, the equilibrium depth of an adsorbed layer, R_e, is approximated by $R_e \simeq aN^{1/2}$. So that for $M = 400\,000$, eq D.2 gives the characteristic time θ in the range $10^0 < \theta < 10^3$ (s).

From the data of Takahashi et al.,[7a] for $M = 400\,000$ and $c_b = 0.3$ g/dL, Γ_e was found to be about 10^{16} monomer/cm^2. On the basis of this, one finds $\gamma_e \cong 4$. With this value of γ_e, eq D.3 predicts a reasonable range of values for t_{int} to be $10^{-1} < t_{int} < 10^2$ (s).

References and Notes

(1) Napper, D. H. *Polymer Stabilization of Colloidal Dispersions*; Academic Press: New York, 1983.
(2) Takahashi, A.; Kawaguchi, M. *Adv. Polym. Sci.* **1982**, *22*, 1.
(3) Cohen-Stuart, M. A.; Cosgrove, V.; Vincent, B. *Adv. Colloid Interface Sci.* **1986**, *24*, 143.
(4) de Gennes, P. G. *Adv. Colloid Interface Sci.* **1987**, *27*, 189.
(5) de Gennes, P. G. In *Molecular Conformation and Dynamics of Macromolecules in Condensed Systems*; Nagasawa, M., Ed.; Elsevier: New York, 1988.
(6) de Gennes, P. G. In *New Trends in Physics and Physical Chemistry of Polymers*; Lee, L. H., Ed.; Plenum: New York, 1989.
(7) (a) Takahashi, A.; Kawaguchi, M.; Hirota, H.; Kato, T. *Macromolecules* **1980**, *13*, 884. (b) Kawaguchi, M.; Hayakawa, K.; Takahashi, A. *Macromolecules* **1983**, *16*, 631.
(8) Israelachvili, J. N.; Tirrell, M.; Klein, J.; Almog, Y. *Macromolecules* **1984**, *17*, 204.
(9) McGlinn, T. C.; Kuzmenka, D. J.; Granick, S. *Phys. Rev. Lett.* **1988**, *60*, 805.
(10) Grant, W. H.; Smith, L. E.; Stromberg, R. R. *Faraday Discuss. Chem. Soc.* **1975**, *59*, 209.
(11) Auvray, L.; Cotton, J. P. *Macromolecules* **1987**, *20*, 202.
(12) Bouchaud, E.; Daoud, M. *J. Phys.* **1987**, *48*, 1991.
(13) de Gennes, P. G. *Macromolecules* **1981**, *14*, 1637.
(14) Kremer, K. *J. Phys.* **1986**, *47*, 1269.
(15) (a) Chakroborty, A. K.; Shaffer, J. S.; Adriani, P. *Macromolecules* **1991**, *24*, 5226. (b) Chakraborty, A. K.; Adriani, P. *Macromolecules* **1992**, *25*, 2470.
(16) (a) Scheutjens, J.; Fleer, G. *J. Phys. Chem.* **1979**, *83*, 1619. (b) Cohen-Stuart, M. A.; Waajen, F. H. W. H.; Cosgrove, T.; Vincent, B.; Crowley, T. *Macromolecules* **1984**, *17*, 1825. (c) Cohen-Stuart, M. A.; Mulder, J. M. *Colloids Surf.* **1985**, *15*, 49.
(17) Varoqui, R.; Pefferkorn, E. *J. Colloid Interface Sci.* **1986**, *109*, 520.
(18) Konash, P. L.; Bastiaans, G. J. *Anal. Chem.* **1980**, *52*, 1929.
(19) Nomura, T.; Minemura, A. *Nippon Kagaku Kaishi* **1980**, *1980*, 1621.
(20) Bruckenstein, S.; Shay, M. *Electrochim. Acta* **1985**, *30*, 1295.
(21) Benje, M.; Eiermann, M.; Pittermann, U.; Weil, K. G. *Ber. Bunsen-Ges. Phys. Chem.* **1986**, *90*, 435.
(22) Hinsberg, W. D.; Wilson, C. G.; Kanazawa, K. K. *J. Electrochem. Soc.* **1986**, *133*, 1448.
(23) Beck, R.; Pittermann, U.; Weil, K. G. *Ber. Bunsen-Ges. Phys. Chem.* **1988**, *92*, 1363.
(24) Kanazawa, K. K. *IBM Res. Rep.* **1989**, RJ6747.
(25) Kanazawa, K. K.; Gordon, J. G. *Anal. Chim. Acta* **1985**, *175*, 99.
(26) Sauerbrey, G. *Z. Phys.* **1959**, *155*, 206.
(27) Benes, E. *J. Appl. Phys.* **1984**, *56*, 608.
(28) Lu, C. In *Applications of Piezoelectric Quartz Crystal Microbalances*; Lu, C., Czanderna, A. W., Eds.; Elsevier: New York, 1984; Chapter 2.
(29) Zimm, B. H. In *Rheology: Theory and Applications*; Eirich, F. R., Ed.; Academic Press: New York, 1960; Vol. 3.
(30) Adam, M.; Delsanti, M. *J. Phys.* **1984**, *45*, 1513.
(31) (a) Fleischer, D. In *Polymer Handbook*; Brandrup, J., Immergut, E. H., Eds.; John Wiley & Sons: New York, 1989. (b) Rudd, J. F. In *Polymer Handbook*; Brandrup, J., Immergut, E. H., Eds.; John Wiley & Sons: New York, 1989.
(32) Flory, P. J. *Principles of Polymer Chemistry*; Cornell University Press: Ithaca, New York, 1967.
(33) Tirrell, M. *Rubber Chem. Technol.* **1984**, *57*, 523.
(34) Durning, C. J.; Tabor, M. *Macromolecules* **1986**, *19*, 2220.
(35) This possibility was suggested by a referee.
(36) (a) Pefferkorn, E.; Carroy, A.; Varoqui, R. *J. Polym. Sci., Polym. Phys. Ed.* **1985**, *23*, 1997. (b) Pefferkorn, E.; Haouam, A.; Varoqui, R. *Macromolecules* **1989**, *22*, 2677. (c) Frantz, P.; Granick, S. *Phys. Rev. Lett.* **1991**, *66*, 899.
(37) Frantz, P.; Leonhardt, D. C.; Granick, S. *Macromolecules* **1991**, *24*, 1868.